6724 *Inorg. Chem.* **2009**, *48*, 6724–6730
DOI: 10.1021/ic900669p

Inorganic Chemistry
Article

Synthesis and Properties of Well-Crystallized Layered Rare-Earth Hydroxide Nitrates from Homogeneous Precipitation

Fengxia Geng,[†,‡] Yoshitaka Matsushita,[§] Renzhi Ma,[†] Hao Xin,[†] Masahiko Tanaka,[§] Nobuo Iyi,[†] and Takayoshi Sasaki*[,†,‡]

[†]*International Center for Materials Nanoarchitectonics, National Institute for Materials Science, 1-1 Namiki, Tsukuba, Ibaraki 305-0044, Japan,* [‡]*Graduate School of Pure and Applied Sciences, University of Tsukuba, 1-1-1 Tennodai, Tsukuba, Ibaraki, 305-8571, Japan, and* [§]*Beamline Station, National Institute for Materials Science, 1-1-1 Kouto, Sayo-cho, Sayo-gun, Hyogo 679-5148, Japan*

Received April 6, 2009

We report the synthesis and characteristics of a rare-earth based layered family, $Ln_8(OH)_{20}(NO_3)_4 \cdot nH_2O$ with Ln = Sm, Eu, Gd, Tb, Dy, Ho, Er, Tm, and Y, synthesized through homogeneous precipitation of $Ln(NO_3)_3 \cdot xH_2O$ with hexamethylenetetramine. The products were uniform and of high crystallinity. Their morphology gradually changed from elongated hexagon (Sm, Eu, Gd) and hexagon (Tb, Dy) to rhombus (Ho, Er, Tm). Selected area electron diffraction revealed that the in-plane structure resembled that of the chloride counterpart, $Ln_8(OH)_{20}Cl_4 \cdot mH_2O$. Unit cell dimensions of the host layer, *a* and *b*, decreased with contracting size of lanthanide ions, whereas no such trend was observed for the interlamellar distance, *c*/2, which is dominated by hydration degree. Stability of the samples with temperature and relative humidity (RH) was examined. At high temperature or low RHs, hydrated water molecules could be removed, which afforded a phase with a basal decrease of ~0.6 Å. The transition was reversible as revealed by an in situ powder X-ray diffraction study, but a RH hysteresis exists. The reversibility increased with an increase in atomic number or layer charge density. Nitrate anions of both phases could be quantitatively exchanged by other anions under ambient conditions.

Introduction

Layered rare-earth hydroxides with the general composition $Ln_8(OH)_{20}(A^{m-})_{4/m} \cdot nH_2O$, wherein A substitutes for an extensive choice of gallery anions such as 2,6-naphthalenedisulfonate, 2,6-anthraquinonedisulfonate, Cl^-, Br^-, NO_3^-, and so forth,[1−4] are gaining increasing awareness as a new addition to rare anion-exchangeable layered host compounds with a range of attractive physical properties anticipated based on lanthanide elements. Layered double hydroxides (LDHs), well-known for their facile anion exchangeability, represent a typical class of anionic clay consisting of positively charged metal hydroxide sheets that are neutralized by the incorporation of exchangeable anions in the interlayer galleries with additional water molecules, and have found applications in a vast variety of fields.[5] Interestingly, the layered rare-earth hydroxides and LDHs have various features in common such as hydroxide-based layered structure and the resultant anion-exchange properties.

The compounds of $Ln_8(OH)_{20}(NO_3)_4 \cdot nH_2O$ (Ln = Gd−Lu, Y, $n \sim 1.5$) have recently been prepared by hydrothermal treatment of their counterpart nitrate salts, $Ln(NO_3)_3 \cdot xH_2O$, and NaOH in the presence of $NaNO_3$.[3] Their anion exchange capability was demonstrated through reaction with a wide range of organic carboxylate and sulfonate anions. The members were extended to Sm and Eu by a careful control on pH conditions.[6] However, knowledge of the nitrates about the evolution trend across the lanthanide series and their stability is still remaining unknown. Furthermore, hydrothermal synthesis in an autoclave generally limits fine control over reactions and large-scale production of samples. Homogeneous precipitation has been proven to be an economic and effective method for growing numerous inorganic

*To whom correspondence should be addressed. E-mail: sasaki.takayoshi@nims.go.jp. Fax: (+81) 29-854-9061.

(1) Gándara, F.; Perles, J.; Snejko, N.; Iglesias, M.; Gómez-Lor, B.; Gutiérrez-Puebla, E.; Monge, M. A. *Angew. Chem., Int. Ed.* **2006**, *45*, 7998.
(2) Geng, F.; Xin, H.; Matsushita, Y.; Ma, R.; Tanaka, M.; Izumi, F.; Iyi, N.; Sasaki, T. *Chem.—Eur. J.* **2008**, *14*, 9255.
(3) McIntyre, L. J.; Jackson, L. K.; Fogg, A. M. *Chem. Mater.* **2008**, *20*, 335.
(4) Poudret, L.; Prior, T. J.; McIntyre, L. J.; Fogg, A. M. *Chem. Mater.* **2008**, *20*, 7447.
(5) Braterman P. S.; Xu Z. P.; Yarberry F. Layered Double Hydroxides (LDHs). In *Handbook of Layered Materials*; Auerbach, S. M., Carrado, K. A., Dutta, P. K., Eds.; Marcel Dekker, Inc.: New York, 2004.
(6) Lee, K.-H.; Byeon, S.-H. *Eur. J. Inorg. Chem.* **2009**, 929.

Published on Web 06/24/2009

compounds, such as LDHs,[7−13] ZnO nanostructures,[14,15] with advantages that include simplicity and easy scale-up because of its production under normal atmospheric pressure. Very recently, we reported the successful synthesis of the chloride family $Ln_8(OH)_{20}Cl_4 \cdot mH_2O$ (Ln = Nd−Tm and Y) through homogeneous precipitation of $LnCl_3 \cdot xH_2O$ using hexamethylenetetramine (HMT) as a hydrolysis agent.[16] All members were isotypic, comprising a positively charged layer of $[Ln_8(OH)_{20}(H_2O)_m]^{4+}$ and Cl^- ions in the interlayer.

Following the previous studies on chlorides, in the present work we report the large-scale synthesis of high-crystalline uniform $Ln_8(OH)_{20}(NO_3)_4 \cdot nH_2O$ (Ln = Sm−Tm and Y) by similar homogeneous precipitation of $Ln(NO_3)_3 \cdot xH_2O$ with HMT. The products across the series are characterized in terms of structure, composition, and morphology. Also, their thermal, hydration, and chemical behaviors are examined and discussed to achieve a deeper understanding of this compound family.

Experimental Section

Materials. All chemicals used in this study were analytical-grade reagents obtained commercially and used without any further treatment. $Ln(NO_3)_3 \cdot xH_2O$ (Ln = La, Ce, Pr, Nd, Sm, Eu, Gd, Tb, Dy, Ho, Er, Tm, Yb, Lu, and Y) were of 99.99% purity from Rare Metallic Co., Japan. $NaNO_3$ and HMT, purity > 99.5%, were from Wako Pure Chemical Co., Japan. Milli-Q filtered water was utilized in all experiments.

Synthesis of $Ln_8(OH)_{20}(NO_3)_4 \cdot nH_2O$. Synthesis was achieved through homogeneous precipitation from an aqueous mixture solution of $Ln(NO_3)_3 \cdot xH_2O$ (5 mmol), $NaNO_3$ (65 mmol), and HMT (5 mol) at a refluxing temperature under nitrogen gas protection for 10 h.[2,16] After air-cooling the system to room temperature, the precipitates were collected by filtration, and washed several times with distilled water and ethanol, followed by drying in a box with humidity set at ∼75%.

Anion-Exchange Reactions of $Ln_8(OH)_{20}(NO_3)_4 \cdot nH_2O$. The as-prepared samples were converted to their Cl^- form by anion-exchange process at room temperature. Typically, samples (0.2 g) were first dispersed in an aqueous solution (200 cm^3) of 1 M NaCl. The reaction vessel was then tightly capped and shaken for 2 days. The identical procedure as described above was used to recover the Cl^--exchanged products.

Instrumentation. Metal contents were determined by inductively coupled plasma (ICP) atomic emission spectroscopy (SPS1700HVR, Seiko Instruments) after dissolving a weighed amount of sample with an aqueous HCl solution. The OH^- content was obtained by titration with 0.1 M standard H_2SO_4 after the sample had been dispersed in water. Carbon content was measured on a LECO CS-444 analyzer. NO_3^- content was quantified with ion chromatography (LC-8020) after dissolving the sample in H_2SO_4. Water content was evaluated by thermogravimetry using a Rigaku TGA-8120 instrument in the temperature range of 25−900 °C at a heating rate of 5 °C min^{-1} under an air flow.

The dimensions and morphology of the samples were examined using a JEOL JSM-6700F field emission scanning electron microscope (FE-SEM). A JEOL JEM-1010 transmission electron microscope (TEM) at an accelerating voltage of 100 kV was employed in TEM observations and selected area electron diffraction (SAED) measurements. The solid sample was dispersed in ethanol by sonication for 5 min, after which a few drops were applied to a TEM carbon-coated copper grid and dried for observation.

High-resolution synchrotron powder X-ray diffraction (XRD) patterns for the Tb sample were recorded on beamline BL15 at the SPring-8 Synchrotron Radiation Facility, Japan (λ=0.65297 Å). The powder sample was packed in a Lindemann capillary tube of 0.5 mm ϕ, and data was collected under ambient conditions. Phase identification was attained based on XRD data collected on a Rigaku RINT Ultima+ diffractometer equipped with graphite-monochromatized Cu Kα radiation (λ = 1.54056 Å) and a humidity-controlled sample chamber. As the samples were very sensitive to humidity, powder XRD patterns were usually recorded at a RH of 75% to preserve their original nature.

In situ powder XRD patterns under controlled RH typically ranging from 5% to 90% were measured to follow sample evolution with RH. The samples were kept at constant humidity for 90 min before recording XRD profiles. Weight change as a function of RH was measured at 25 °C on a Rigaku ThermoPlus TG8120 by introducing the RH-controlled N_2 atmosphere at 1 dm^3/min. The samples were initially kept at RH of ∼90% for 1−2 h to reach equilibration, and then the weight was recorded after 30 min of holding at each 10% decrease in RH. Reversibility of the humidity-triggered change was also studied using both XRD and gravimetry in a cycle of decreasing RH from 90% to 5% followed by increasing to 90% in steps of 10%.

Excitation and emission spectra of the samples were measured on a Hitachi F-4500 fluorescence spectrophotometer at room temperature.

Results and Discussion

Synthesis and Characterization of $Tb_8(OH)_{20}(NO_3)_4 \cdot 7.2H_2O$. Synthesis was started by dissolving nitrate salt ($Ln(NO_3)_3 \cdot xH_2O$) and HMT in the presence of $NaNO_3$ in water, followed by refluxing the mixture solution for 10 h. Precipitates were formed after being heated for about 1 h with crystallinity improved by extending the reaction period (Supporting Information). An identical phase could also be yielded without addition of $NaNO_3$, but product quality was relatively lower. On the basis of element analysis results, the chemical composition of the so-obtained Tb sample was estimated to be $Tb(OH)_{2.45}(NO_3)_{0.50}(CO_3)_{0.025} \cdot 0.9H_2O$ (Anal. Calcd (%) Tb, 63.7; OH, 16.7; NO_3, 12.4; CO_3, 0.6; H_2O, 6.5. Found (%): Tb, 63.7; OH, 16.7; NO_3, 12.3; CO_3, 0.5; H_2O, 6.5). For simplicity, the carbonate charge was normalized to hydroxyls as $Tb(OH)_{2.5}(NO_3)_{0.50} \cdot 0.9H_2O$. The composition is consistent with that prepared by hydrothermal method ($Tb(OH)_{2.5}(NO_3)_{0.50}$ $0.75H_2O$),[3] except that the hydration degree is higher, which may have resulted from our efforts to avoid overdrying during both the sample collection and drying process. The Tb/OH molar ratio equals that of the recently reported hydroxide chloride series $Ln_8(OH)_{20}Cl_4 \cdot mH_2O$,[16] suggesting a close relationship that is addressed later.

(7) Li, L.; Ma, R.; Ebina, Y.; Iyi, N.; Sasaki, T. *Chem. Mater.* **2005**, *17*, 4386.
(8) Liu, Z.; Ma, R.; Osada, M.; Takada, K.; Sasaki, T. *J. Am. Chem. Soc.* **2005**, *127*, 13869.
(9) Ma, R.; Liu, Z.; Takada, K.; Iyi, N.; Bando, Y.; Sasaki, T. *J. Am. Chem. Soc.* **2007**, *129*, 5257.
(10) Iyi, N.; Matsumoto, T.; Kaneko, Y.; Kitamura, K. *Chem. Lett.* **2004**, *33*, 1122.
(11) Ogawa, M.; Kaiho, H. *Langmuir* **2002**, *18*, 4240.
(12) Benito, P.; Herrero, M.; Barriga, C.; Labajos, F. M.; Rives, V. *Inorg. Chem.* **2008**, *47*, 5453.
(13) Jobbágy, M.; Blesa, M. A.; Regazzoni, A. E. *J. Colloid Interface Sci.* **2007**, *309*, 72.
(14) Vayssieres, L. *Adv. Mater.* **2003**, *15*, 464.
(15) Li, Q. C.; Kumar, V.; Li, Y.; Zhang, H. T.; Marks, T. J.; Chang, R. P. H. *Chem. Mater.* **2005**, *17*, 1001.
(16) Geng, F.; Matsushita, Y.; Ma, R.; Xin, H.; Tanaka, M.; Izumi, F.; Iyi, N.; Sasaki, T. *J. Am. Chem. Soc.* **2008**, *130*, 16344.

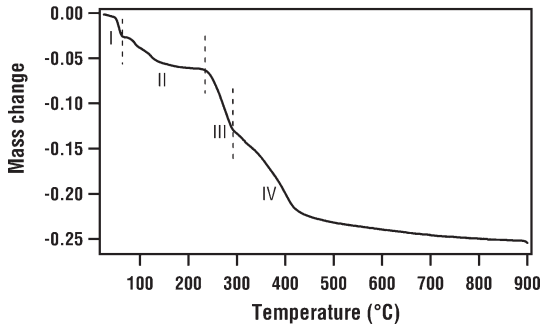

Figure 1. TG curve for $Tb_8(OH)_{20}(NO_3)_4 \cdot 7.2H_2O$.

The thermal gravimetry (TG) measurement is in reasonable agreement with the composition. Figure 1 shows the TG curve of the Tb sample in the temperature range of 25−900 °C. The compound underwent weight loss of 26.2% in four steps. Initial removal of water molecules is observed up to 60 °C, accompanied by a basal spacing contraction, corresponding to a low-hydrated phase that is addressed in detail later. Complete loss of solvent occurs between 60 and 220 °C with total weight loss of 6.2%, close to the value of 6.5% calculated for the loss of 0.9 mol of water molecules per chemical formula unit. The low-hydrated phase seems to be thermally robust in this range with nearly constant basal spacing, suggesting the low-hydrated phase is stabilized by the initial water loss. The subsequent sharp weight loss of 6.8% in the temperature range of 220−290 °C can be attributed to the release of water from dehydroxylation of the hydroxide layers. The final step starting from 290 °C is assigned to the further decomposition of the compound, combustion of anionic ions. The final residue product was Tb_4O_7. XRD patterns of samples after each stage are provided in Supporting Information.

The size and morphology of the products were examined by TEM. As shown in Figure 2a, a typical TEM image for the Tb sample displayed quasi-hexagonal platelike morphology with side length of about 2 μm; especially, it appeared more uniform in shape and size than that from hydrothermal synthesis reported recently.[3] The angles were sharp at 120°, suggesting high crystallinity. The uniformity and high crystallinity of the products can be attributed to the homogeneous and slow nucleation process throughout the solution utilizing HMT hydrolysis. Electron diffraction pattern taken on a single platelet further confirmed the single-crystalline nature of the sample. It is noteworthy that the diffraction pattern was the same as that for the chloride counterpart, indicating similar in-plane structure. The bright spots likely originate from the quasi-hexagonal network of rare-earth cations viewed along the layer normal, while weaker spots, indexed as 100 and 010, are a sort of superlattice reflection related to the slight deviation from a perfect hexagonal arrangement.[2] The in-plane parameters were estimated as $a \sim 12$ Å, $b \sim 7$ Å.

The highly crystalline nature with well-ordered and regular stacking sequence was further confirmed by the XRD results. The high-resolution synchrotron-radiated XRD profile is shown in the Supporting Information. Harmonic reflections, 00*l*, were especially strong compared with a large number of non-basal peaks, indicating

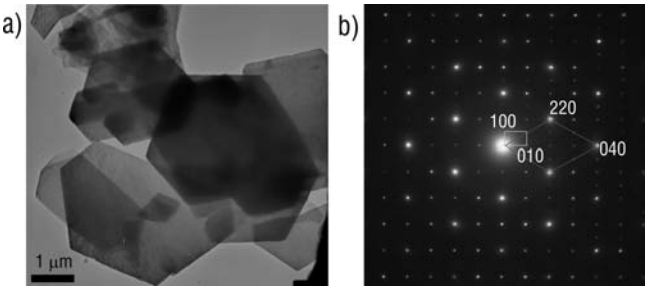

Figure 2. (a) Typical TEM image of $Tb_8(OH)_{20}(NO_3)_4 \cdot 7.2H_2O$ displaying uniform quasi-hexagonal platelets with high crystallinity. (b) SAED pattern on one platelet in (a) taken along the [001] zone axis.

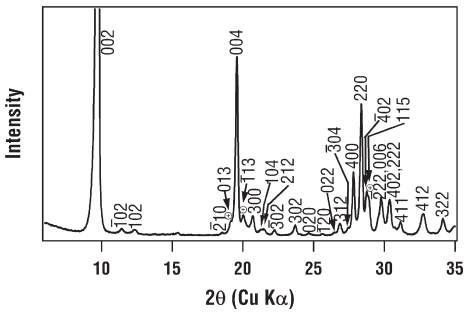

Figure 3. XRD pattern for $Tb_8(OH)_{20}(NO_3)_4 \cdot 7.2H_2O$ ($\lambda = 1.5405$ Å). The pattern was indexed as a monoclinic cell $a = 12.865(6)$ Å, $b = 7.208(3)$ Å, $c = 18.18(2)$ Å, $\beta = 94.45(9)°$. The mark ⊕ represents reflections that cannot be incorporated in a single-layer repetition cell.

a well-developed layered structure with a stacking distance of 9.1 Å. Interlayer spacing together with *a* and *b* parameters from TEM characterization (vide ante) were used to index the pattern, from which we deduced a monoclinic unit cell: $a = 12.865(6)$ Å, $b = 7.208(3)$ Å, $c = 18.18(2)$ Å, $\beta = 94.45(9)°$. The indexing below 35° is shown in Figure 3. The presence of an extremely large number of peaks and their overlaps in the high-angle area prevented accurate identification. The cell is close to the one proposed in an earlier study[3] except for a difference in axis notation. Doubling the basal spacing to the *c*-axis was involved because some of the peaks, marked with ⊕, could only be incorporated in the unit cell containing two metal hydroxide layers. The incorporation of two layers in the unit cell is indicative of the possible relative displacement of adjacent slabs with respect to each other or different directions of nitrate anions in neighboring galleries. It is notable that unit-cell dimensions of the monoclinic $Tb_8(OH)_{20}(NO_3)_4 \cdot 7.2H_2O$ are closely related to those of orthorhombic chloride counterpart $Tb_8(OH)_{20}Cl_4 \cdot 7.0H_2O$, for which the cell was $a = 12.8027(4)$ Å, $b = 7.2560(2)$ Å, $c = 8.4436(5)$ Å. In-plane parameters, *a* and *b*, of the two are very similar. Together with the discussion above on TEM, it is thus reasonable to conclude that the lamellar phase described here presents a structure analogous to that of $Tb_8(OH)_{20}Cl_4 \cdot 7.0H_2O$, layers of $[Tb_8(OH)_{20}(H_2O)_{7.2}]^{4+}$ parallel to (001) accommodating charge-balancing anions of NO_3^-. Hydroxide and water molecules of the host layers are bridged by interlayer anions and water molecules by electrostatic interaction and hydrogen bonding. Close examination of the indices suggests a systematic absence of $l = 2n + 1$ for *h*0*l*, which indicates possible

space groups of *Pc*, $P2/c$, $P2_1/c$. However, the successful determination of the structure has been hindered by severe overlapping of the powder data.

Extension to Other Lanthanides. The size of lanthanide ions decreases monotonically, known as lanthanide contraction, and accordingly, the physical and chemical properties of lanthanide compounds demonstrate gradual variation on ascending the series. Previous studies on lanthanide compounds such as hydroxides, phosphates, fluorides, and so on, indicate that crystal structure and morphology change gradually with decreasing radii.[17−19] In our case, the as-prepared products under similar conditions adopt three different kinds of crystal structures (Supporting Information). The desired $Ln_8(OH)_{20}(NO_3)_4 \cdot nH_2O$ could be obtained as a single phase for intermediate lanthanides from Sm to Tm and Y. Two sets of basal spacing, 8.8 and 8.4 Å, observed for Sm, are not due to any byproduct. The origin is detailed in a later section. Under the same conditions, larger lanthanides (La, Ce, Pr, Nd) could only yield a hexagonal phase of $Ln(OH)_3$. Since Ce^{3+} is very easily oxidized, CeO_2 was occasionally obtained (Supporting Information). On the other hand, some unidentified phase was formed with smaller Ln^{3+} ions (Yb and Lu). The variation in crystal structure is considered to be related to the gradual radius contraction of Ln^{3+}. Notably, members in the nitrate family using a hydrothermal method under the same synthesis conditions were limited to elements smaller than Gd; larger Ln elements only gave a mixture of $Ln(OH)_2(NO_3) \cdot xH_2O$ ($x = 0$ and 1) and $Ln(OH)_3$ and a second phase coexisted in the smallest lanthanide cases, Yb and Lu.[3] In the present synthesis, the diffraction patterns of lanthanides from Sm to Tm and Y were consistent with that of the Tb sample and did not indicate traces of $Ln(OH)_2(NO_3) \cdot xH_2O$ or $Ln(OH)_3$. XRD peaks of all samples below 35° are sharp and symmetric, which proves their higher crystallinity, while peaks at the high-angle area are apparently broad because of the overlapping of a large number of peaks. Unit-cell dimensions refined with an indexing program (APPLEMAN)[20] along with their layer charge density are listed in Table 1. In-plane dimensions, *a* and *b*, show the expected decreasing trend with increasing atomic number of Ln, which corresponds to the decreasing size from early to late Ln^{3+} ions, and the layer charge density increases consequently. However, there is no such trend for the interlamellar distance, $c/2$, which could be rationalized by its high sensitivity to hydration degree. The same trend was observed in the chloride series $Ln_8(OH)_{20}Cl_4 \cdot mH_2O$ (Ln = Nd−Tm and Y) with in-plane lattice parameters, *a* and *b*, decreasing with increasing atomic number, and the interlamellar distance, *c*, depending on hydration.[16]

TEM and SEM characterization provide further details on the morphology and structure of this compound series. As revealed by SEM images (Supporting Information), all members adopted platelet morphology and their size was rather uniform. It is interesting to find that their lateral size tends to be reduced with the increase in atomic number. Typical TEM images of the as-prepared Gd, Dy, and Er samples are shown in Figures 4a−c. Under similar experimental conditions, platelets of lighter Sm, Eu, and Gd samples were crystallized in an elongated hexagon with side length of approximately 20 and 5 μm (Figure 4a), respectively, which gradually decreased to

Table 1. Lattice Parameters and Layer Charge Density (ξ) of $Ln_8(OH)_{20}(NO_3)_4 \cdot nH_2O$ Materials Obtained from Conventional XRD Data

Ln	*a* (Å)	*b* (Å)	*c* (Å)	β (deg)	ξ (10^{-2}/Å^2)
Sm[a]	13.070(5)	7.362 (3)	18.12 (4)	94.64(5)	4.16
Eu	13.004(6)	7.304(4)	18.15(2)	94.68(8)	4.21
Gd	12.933(4)	7.249(2)	18.155(6)	94.84(4)	4.27
Tb	12.865(6)	7.208(3)	18.18(2)	94.45(9)	4.31
Dy	12.778(6)	7.158(3)	18.215(8)	93.74(5)	4.37
Ho	12.721(3)	7.132(4)	18.347(9)	92.98(5)	4.41
Er	12.660(6)	7.095(4)	18.37(1)	94.21(7)	4.45
Tm	12.647(3)	7.062(2)	18.426(7)	94.64(4)	4.48
Y	12.741(9)	7.135(3)	18.35(1)	93.73(7)	4.40

[a] The larger basal spacing was used for refinement.

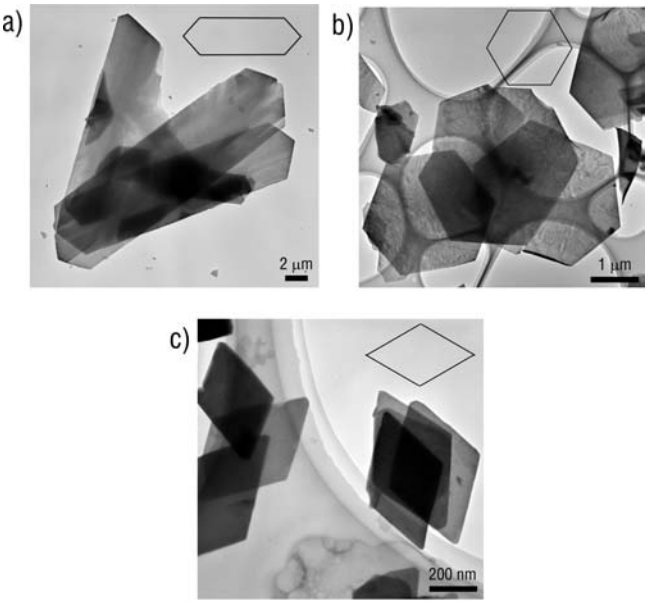

Figure 4. Typical TEM images of three morphologies for large (Sm, Eu, Gd), intermediate (Tb, Dy) and small lanthanides (Ho, Er, and Tm). (a) Gd elongated hexagon, (b) Dy hexagon, and (c) Er rhombus platelets. The insets illustrate the typical geometry of sample platelets.

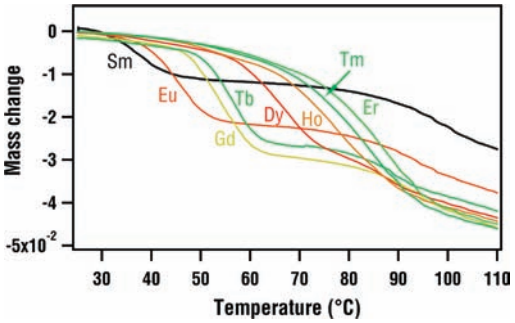

Figure 5. TG profiles of $Ln_8(OH)_{20}(NO_3)_4 \cdot nH_2O$ for first step water evaporation (Ln = Sm, Eu, Gd, Tb, Dy, Ho, Er, and Tm).

(17) Wang, X.; Li, Y. D. *Angew. Chem., Int. Ed.* **2002**, *41*, 4790.
(18) Yan, R. X.; Sun, X. M.; Wang, X.; Peng, Q.; Li, Y. D. *Chem.—Eur. J.* **2005**, *11*, 2183.
(19) Li, C. X.; Yang, J.; Yang, P. P.; Lian, H. Z.; Lin, J. *Chem. Mater.* **2008**, *20*, 4317.
(20) Appleman, D. E.; Evans, H. T.; Handwerker, D. S. *Program X-ray*; Geological Survey, U.S. Department of the Interior: Washington, DC, 1966.

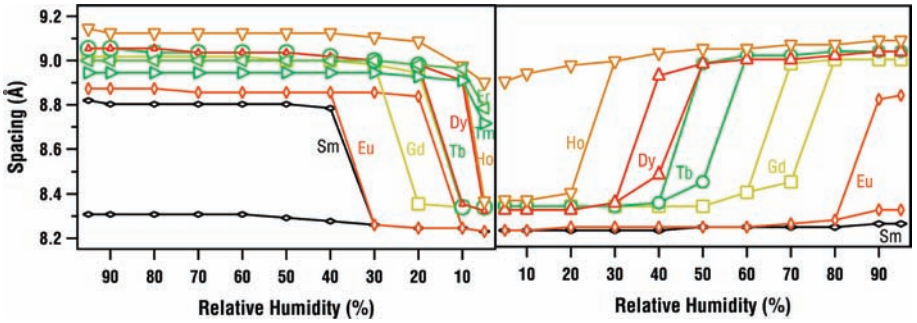

Figure 6. Changes in basal spacing with RH for nitrate series. The left and right panels correspond to the change with decrease in humidity and subsequent increase, respectively.

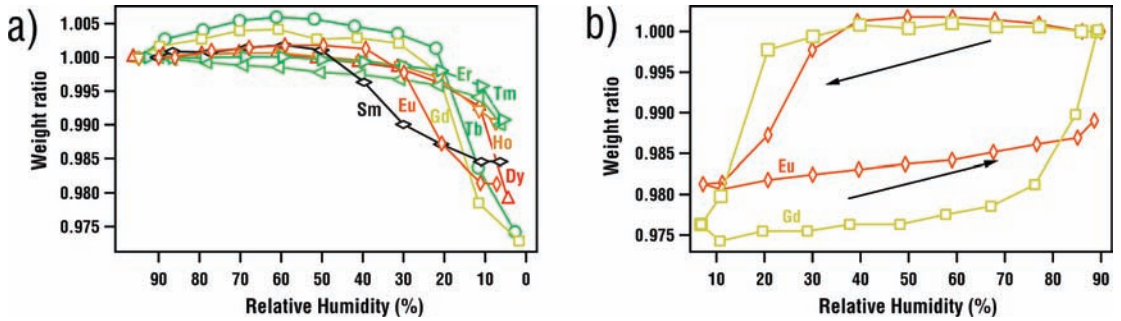

Figure 7. Change in weight with RH (a) decreasing from 95% to 5% at steps of 5% and (b) in a cycle decreasing from 90% to 5% followed by increasing to 90%.

1−2 μm for Tb and Dy (Figure 4b), while a rhombus morphology was taken for those of heavier lanthanides (Figure 4c) with size of 2 μm for Ho, and hundreds of nanometers for Er and Tm. This is different from the chloride series, in which light lanthanides (Nd, Sm, Eu) grew into rectangular platelets, whereas platelets of heavy lanthanides from Gd tended to be of quasi-hexagonal morphology with similar size. SAED patterns of all members recorded perpendicular to the platelets were the same as that of the Tb sample (not shown), thus suggesting their structural analogy.

Thermal Stability. The thermal stability of all compounds was studied using thermal gravimetric analysis as provided in Figure 5. All compounds exhibited very similar mass loss over the entire operating range (Supporting Information). As detailed in the Tb sample, complete water loss of about 6% was observed up to 230 °C. The dehydroxylation and combustion of anions occurs between 230−290 °C and 290−600 °C before the samples reach a plateau. It is interesting to note that the temperature for first step water evaporation and the corresponding weight loss increased from left to right lanthanides, suggesting enhancement of the stability of coordinated water and the ability to incorporate water molecules with increasing atomic number. The temperature range was approximately 25−45 °C for Sm, 30−55 °C for Eu, 40−65 °C for Gd and Tb, 50−75 °C for Dy, and 60−95 °C for Ho, Er, and Tm although precise data was difficult to read. This tendency is contrary to that observed in the chloride family, the hydration capability of which typically decreased, or water deficiency increased, with the increase in atomic number from Nd to Tm. Hydrogen bonding to the anions was found to play an important role in stabilizing the cage around trivalent

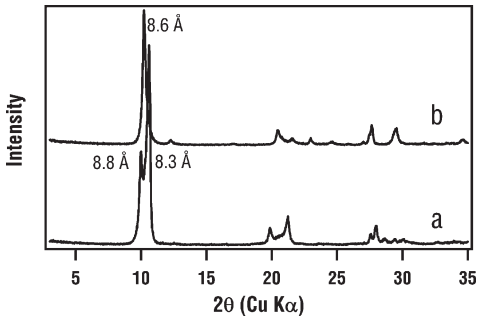

Figure 8. XRD patterns of (a) the nitrate precursor and (b) Cl^--exchanged products of the Sm sample.

metal cations and the hydration number is less in compounds with weaker hydrogen bonds;[21] therefore, the more limited hydrogen-bonding ability of nitrate ion arising from its nonspherical electron distribution[22] may, in turn, contribute to the difference and facilitation of water loss.

Variation in Basal Spacing with RH. An abrupt basal spacing shrinkage of ~0.2 Å was observed at critical RH for some members of the chloride family, which proved to be from the loss of some coordinated water molecules at low RH.[16] Similarly, the nitrate family is also sensitive to humidity conditions. The phases adopted at high and low RH are hereafter referred to as high-hydrated (HH) and low-hydrated (LH) phase, respectively. Changes in basal spacing with RH decreasing from 95% to 5% of all members, followed by rehydration to 95% to examine

(21) Abbasi, A.; Lindqvist-Reis, P.; Eriksson, L.; Sandström, D.; Lidin, S.; Persson, I.; Sandström, M. *Chem.—Eur. J.* **2005**, *11*, 4065.
(22) Haschke, J. M. *Inorg. Chem.* **1974**, *13*, 1812.

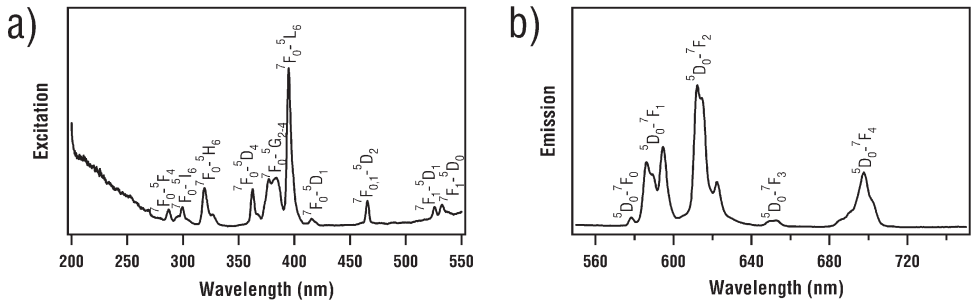

Figure 9. Room-temperature (a) excitation and (b) emission spectra of $Eu_8(OH)_{20}(NO_3)_4 \cdot 7.2H_2O$ monitored around 612 nm and excited at 395 nm.

reversibility, are presented in Figure 6. According to their behavior, the series can be divided into three subgroups intersecting at Sm and Ho. (I) Sm: dehydration−rehydration process is irreversible, HH ⇄ LH. The two sets of basal reflections, 8.8 and 8.3 Å, for the largest lanthanide successfully incorporated, Sm, correspond to HH and LH phases, respectively. At RH of 30%, the HH component completely converted to LH, whereas subsequent rehydration did not bring about any signs of basal expansion. (II) Eu, Gd, Tb, Dy, and Ho: dehydration−rehydration process is reversible, HH ⇄ LH; however, markedly distinct from the promptly reversible basal change in the chloride series, RH hysteresis was found and the degree of hysteresis diminished with increasing charge density/atomic number. Upon decreasing RH to a critical value, LH phases were discerned. RH for emergence of LH phase became lower with increasing atomic number, that is, 30%, 20%, 10%, 10%, and 5% for Eu, Gd, Tb, Dy, and Ho samples, respectively, suggesting increasing stability in HH phases from early to late lanthanides. Further dehydration led to complete conversion to LH phase. The stability increase is also reflected in the high probability of phase restoration back to its nascent form by rehydration, with the RH threshold for abrupt basal expansion also decreasing with increasing atomic number, for example, RH of 90%, 70%, 50%, 40%, and 30% for Eu, Gd, Tb, Dy, Ho samples, respectively. Continued rehydration afforded an increase in HH phase fractions judging from the relative intensity of basal reflections of the two phases, and finally completed restoration except for the larger lanthanide Eu sample, which only showed partial reversion with LH phase still remaining at the highest experimental RH of 95%. (III) Er and Tm: HH phase was adopted throughout the humidity range of 5% to 95%. No trace of LH phase was observed even when suction filtration was used to collect the samples. The above studies demonstrate that high layer charge density favors HH phase with better HH−LH conversion reversibility, consistent with the TG study.

The humidity-dependent behavior was further corroborated by gravimetry. Weight change in all members with respect to RHs, indicated in ratios relative to the weight at RH = 90%, are provided in Figure 7a. Their behavior concurs well with XRD observations. Sm, Eu, Gd, Tb, and Dy samples exhibited consistent abrupt weight loss at RH 40%, 20%, 10%, 10%, and 5%, respectively. No appreciable weight decrease was observed for Ho, Er, and Tm samples. Figure 7b depicts the weight reversibility of Eu and Gd samples. Obviously, although the weight of the Eu sample increased with increasing humidity, the weight was not completely recovered at RH 90%, which agrees well with the fact that the sample was still a mixture of HH and LH phases in XRD measurements. For the Gd sample, the weight was regained, but there was a large hysteresis. Thus, the samples were very sensitive to RH, and it is essential to pay special attention to humidity during the collection process (Supporting Information).

Anion-Exchange of $Ln_8(OH)_{20}(NO_3)_4 \cdot nH_2O$. The anion exchangeability of $Ln_8(OH)_{20}(NO_3)_4 \cdot nH_2O$ (Ln = Gd−Tm) of larger basal spacing (HH phases)[3] and $Ln_8(OH)_{20}(NO_3)_4 \cdot nH_2O$ (Ln = Sm, Eu, Gd) of smaller spacing (LH phases)[6] from hydrothermal reactions was demonstrated through reactions with a wide range of anions. Here, anion-exchange reactions across the series $Ln_8(OH)_{20}(NO_3)_4 \cdot nH_2O$ (Ln = Sm, Eu, Gd, Tb, Dy, Ho, Er, and Tm) were performed by conventional anion-exchange procedure at room temperature and spherical Cl^- anion was chosen for discussion. Figure 8 compares the XRD pattern of the Sm-based nitrate sample with one after being exchanged to Cl^-. Only one set of basal reflections corresponding to 8.6 Å could be observed after the exchange, in contrast to the presence of two sets, 8.8 Å and 8.3 Å, in the nitrate precursor. From the initial basal spacing of ~8.9 Å of pristine NO_3^--intercalated products, the values for Eu- and Gd-based intercalated products shifted to 8.7 Å and Tb, Dy, Ho, Er, and Tm samples to 8.3 Å, comparable to directly synthesized Cl^- intercalated samples (Supporting Information). The peak positions of all reflections in the patterns matched well with those of the patterns for the directly precipitated chloride samples. These results suggest that both HH and LH phases are anion exchangeable. Peaks of all samples except Tm were sharp and symmetric, clearly indicating that the well-ordered and regular stacking sequence was preserved during the exchange process.[23] Also, Eu and Tb samples exhibited typical Eu^{3+} red and Tb^{3+} green emission, indicating that the materials might be promising candidates for luminescence devices. Figure 9 shows the room-temperature excitation and emission spectra of Eu sample (For details, see Supporting Information).

Conclusions

We have demonstrated that homogeneous precipitation of $Ln(NO_3)_3 \cdot xH_2O$ with HMT is an effective way to synthesize a uniform and high-crystalline layered family with the

(23) The broadening of basal reflections of the Tm sample could originate from the coexistence of another phase from its small cationic size, as illustrated in the chloride series.

composition $Ln_8(OH)_{20}(NO_3)_4 \cdot nH_2O$ (Ln = Sm, Eu, Gd, Tb, Dy, Ho, Er, Tm, and Y). Structural study indicated that the nitrate family is closely related to its chloride counterpart, $Ln_8(OH)_{20}Cl_4 \cdot mH_2O$. Unit-cell dimensions of the two are similar except that nitrate is in monoclinic symmetry with $\beta \sim 94°$ and the interlamellar dimension, c, involves doubling. In-plane lattice parameters, a and b, show the expected decrease with decreasing size of lanthanide ions.

The samples undergo contraction of interlayer spacing and convert to LH phases with decreasing RH or increasing temperature, corresponding to the removal of partial water molecules. The LH phases can typically be rehydrated to their nascent form at high RH. The stability of HH phases and reversibility with RH increases with increasing layer charge density or atomic number. Anion-exchange study showed that both HH and LH phases can undergo anion-exchange reactions under ambient conditions. Beyond the exchangeability of anions, the Eu and Tb compounds can serve as useful phosphors.

Acknowledgment. This work was supported by World Premier International Center Initiative (WPI Initiative) on Materials Nanoarchitectonics, MEXT, Japan and CREST of the Japan Science and Technology Agency (JST).

Supporting Information Available: Synchrotron XRD pattern of Tb sample, more XRD patterns, SEM images, TGA curves, and photoluminescence properties of Eu and Tb samples. This material is available free of charge via the Internet at http://pubs.acs.org.